Rapid, Large-Scale Synthesis and Electrochemical Behavior of Faceted Single-Crystalline Selenium Nanotubes

Sheng-Yi Zhang,[†,‡] Yi Liu,[†] Xiang Ma,[§] and Hong-Yuan Chen*[,†]

Key Laboratory of Analytical Chemistry for Life Sciences, School of Chemistry and Chemical Engineering, Nanjing University, Nanjing 210093, China, Department of Chemistry, Anhui University, Hefei 230039, China, and Center for Instrumental Analysis, Nanjing University, Nanjing 210093, China

Received: November 20, 2005; In Final Form: January 26, 2006

This article describes a rapid, solution-phase approach to the large-scale synthesis of faceted single-crystalline Se nanotubes, in the presence of cetyltrimethylammonium bromide. The products were characterized by scanning electron microscopy, high-resolution transmission electron microscopy, X-ray diffraction, X-ray photoelectron spectroscopy, laser Raman spectrography, differential scanning calorimetry analysis, and thermogravimetric analysis. The growth mechanism of the Se nanotubes was investigated by a series of experiments, and the rationality of the faceted morphology model for the Se nanotubes was demonstrated from the energetics and geometry. Furthermore, the electrochemical behavior of the Se nanotubes was studied by voltammetric techniques.

Introduction

Since carbon nanotubes were discovered by Iijima,[1] more and more attention has been attracted to the synthesis of nanotubes, owing to their intriguing nanotubular structures, interesting properties, and promising applications. In recent years, besides carbon nanotubes, nanotubes consisting of other materials have been created, such as TiO_2,[2] Sb_2O_3,[3] Te,[4] Mn_5Si_3,[5] MoS_2,[6] CdS,[7] V_2O_5,[8] Cu,[9] and AlN.[10]

Selenium, as a member of the semiconductor family, has many important physical properties, such as high piezoelectricity, high photoconductivity, superconductivity, thermoelectricity, and nonlinear optical responses, and has wide applications in various fields, such as rectifiers, solar cells, photographic exposure meters, and xerography.[11] Therefore, it is reasonable to expect that the unique structures and properties of Se nanoparticles, especially one-dimensional (1D) Se nanostructures, will enhance the performance of existing devices or introduce new applications. For example, 1D Se nanostructures can be expediently used to construct nanoscale optoelectronic devices due to their excellent optoelectronic characteristics[12] and used as the chemical templates to produce other functional materials due to their high reactivity toward a variety of chemicals.[13,14] Recently, a number of synthetic strategies have been applied to prepare Se nanowires and nanorods.[15−22] The reports on the synthesis of Se nanotubes are, however, relatively few. Last year, Zhang and co-workers prepared Se nanotubes using a hydrothermal process.[23] Ma and co-workers obtained Se nanotubes by dismutation of Na_2SeSO_4 in a $C_{12}E_{23}$ micelle system.[24] This year, Li and co-workers produced Se nanotubes with a sonochemical method.[25] In our previous work, a few Se nanotubes were prepared by an electrochemical approach.[26] These methods usually take a longer time to obtain appreciable quantities of Se nanotubes. Obviously, developing effective routes to fabricate large quantities of Se nanotubes at a low cost is challenging. Herein, we present a controllable and rapid approach to the large-scale synthesis of faceted Se nanotubes in a highly concentrated cetyltrimethylammonium bromide (CTAB) solution. Furthermore, the electrochemical behavior of the as-prepared Se nanotubes was studied. The redox characteristics of the Se nanotubes, which are significant in a variety of diverse fields,[27,28] were examined.

Experimental Section

Synthesis. All of the reagents are of analytical grade and were used without further purification. Typically, the synthesis was carried out as follows. First, 22.5 mL of 2.0 M selenious acid (H_2SeO_3) was added into 100 mL of 0.3 M CTAB in a 200 mL flask placed in a water bath at 70 ± 0.5 °C. Then, 2.5 mL of 80% hydrazine (N_2H_4) was dropwise added into the selenious acid/CTAB solution under ultrasonic irradiation (in a KQ3200 ultrasound apparatus, 120 W, 40 kHz, Kunshan Co., China). After ultrasonication for 5 min, the reaction mixture was aged in a water bath at the given temperature for 3 h. The final product was centrifuged, washed by alcohol and deionized water several times, and dried at room temperature under reduced pressure. It should be pointed out that the Se samples could not be discarded to the environment because excessive Se is toxic.

Characterization. Pictures of the CTAB solution were taken by inverted fluorescence microscopy (IFM, Leica Dmire2, Germany). The product was characterized by scanning electron microscopy (SEM) with an energy-dispersive X-ray analysis (EDAX, Philips XL30 ESEM and Hitachi X-650 SEM), transmission electron microscopy (TEOL JEM-100SX TEM), high-resolution transmission electron microscopy (HRTEM, Philips CM200 FEG TEM, with a high voltage of 200 kV), X-ray photoelectron spectroscopy (XPS, ESCA 3 Mk II, VG Scientific, U. K., equipped with a Mg Kα 1253.6 eV) X-ray source, X-ray diffraction (XRD, Japan Rigaku D/max-RA X-ray diffractometer, with graphite monochromatized Cu $K\alpha_1$ radiation, $\lambda = 0.15406$ nm), and laser Raman spectrography (LRS,

* Author to whom correspondence should be addressed. Phone/Fax: +86 25 8359 4862. E-mail: hychen@nju.edu.cn.
[†] Department of Chemistry, Nanjing University.
[‡] Department of Chemistry, Anhui University.
[§] Center for Instrumental Analysis, Nanjing University.

10.1021/jp056718o CCC: $33.50
Published on Web 04/14/2006

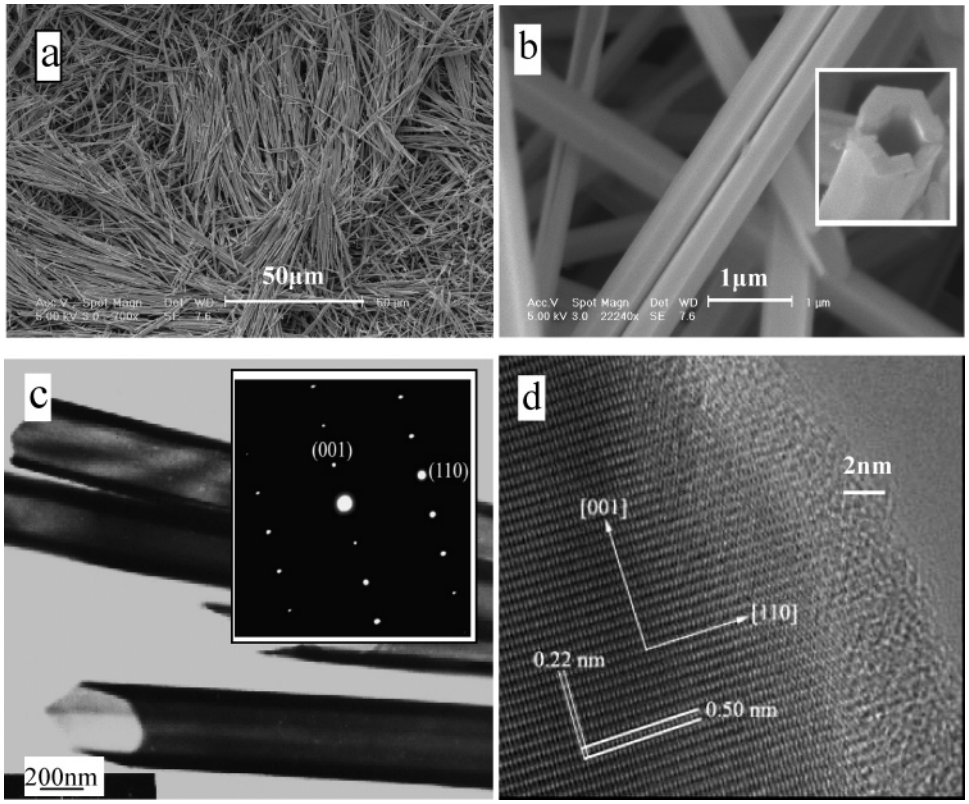

Figure 1. Characterization of the product obtained with a typical experiment. (a) SEM image. (b) Enlarged SEM image. The insert shows the hexangular mouth of a nanotube. (c) TEM image. The insert shows a typical electron diffraction pattern taken from an individual Se nanotube. (d) HRTEM image obtained from the edge of an individual nanotube.

JY HR800, equipped with a 488 nm, 10 mW argon ion laser). The thermogravimetric (TG) analysis and differential scanning calorimetric analysis (DSC) were carried out on a TG/DSC apparatus (Pyris-1, Perkin-Elmer, at a heating rate of 20 °C/min in flowing high-purity nitrogen gas with 20 mL/min).

Electrochemistry. The electrochemical behavior of the product was studied on an electrochemical working station (CHI660A). The cell was made up of a platinum sheet counter electrode, a calomel (saturated) reference electrode against which all potentials were recorded, and a working electrode that was prepared as follows. A little product dispersed in 1% Nafion alcohol solution was spread on a glassy carbon electrode surface and dried at ambient temperature. The electrolyte solution was degassed with ultrapure N_2 prior to experiment. The potential sweep rate was 1.0 mV/s for all electrochemical experiments.

Results and Discussion

Characterization. The SEM image (Figure 1a) of the product displays exclusively 1D nanostructures with the lengths ranging from several tens to ca. 100 μm. The tubular characteristics of the 1D nanostructures with uniform diameter can be clearly seen in an enlarged SEM image (Figure 1b). The TEM image (Figure 1c) shows that the hollow nanotubes are typically 40 nm in thickness of walls and 300 nm in diameter. The selected area electron diffraction (ED) pattern (inserted in Figure 1c) manifests itself in sharp spots, implying the single crystallinity of the nanotube. Noteworthily, such a tubular product can be obtained on a large scale (about 3.0 g, useful output 84.5%) with a typical experiment. The HRTEM image (Figure 1d) gives further insight into the details of the crystal structure of the nanotube. The clear lattice fringes in the HRTEM image show that the nanotube is highly crystalline. The fringe spacings (0.50 and 0.22 nm) observed in this image agree well with the interplanar spacings of the (001) and (110) lattice planes of trigonal Se (t-Se), respectively, which also indicates that the nanotube is a single crystal grown along the *c*-axis.[29]

The EDAX (Figure 1S in the Supporting Information) of the product indicates that the nanotubes are composed of pure Se, and the XPS of the product confirms that Se is in its elemental state since the electron binding energy of Se 3d is 54.9 eV (as shown in Figure 2a), which corresponds to that of the Se(0),[30] whereas the electron binding energies of Se 3d for Se(−II), Se(+IV), and Se(+VI) are ca. 53 eV,[31] 59 eV,[32] and 61 eV,[33] respectively.

The crystallization and purity of the Se nanotubes were further studied by a series of measurements. The LRS pattern taken from the Se nanotubes is shown in Figure 2b. An intensive resonance peak at 234.8 cm^{-1} is assigned to the stretching mode (A1) of a chainlike structure that only exists in the t-Se phase.[29] The narrow half-width (5 cm^{-1}) of this peak suggests that the Se nanotubes have a highly crystalline quality. The peaks at 436.6 and 447.0 cm^{-1} are the second-order spectra of t-Se,[34] and the peak at 140.8 cm^{-1} is the transverse optical phonon mode.[25] In addition, the characteristic Raman peaks at 256 and 264 cm^{-1}, belonging to monoclinic Se and a-Se respectively,[16] do not appear. Figure 2c provides a typical XRD pattern recorded in the 2θ range of 20−80° at a scanning rate of 10°/min. All of the diffraction peaks in the XRD pattern can be readily indexed to crystalline t-Se. The lattice constants (a = 0.435 nm, c = 0.496 nm) calculated from this XRD pattern correspond well to those (a = 0.436 nm, c = 0.495 nm) of the trigonal phase reported in the literature.[35] Obviously, these two constants also agree well with the fringe spacings (0.22 and 0.50 nm) observed in the HRTEM image (Figure 1d), only noticing that the *a*-axis constant is twice as much as the spacing of the (110) planes and the *c*-axis constant is equal to the spacing

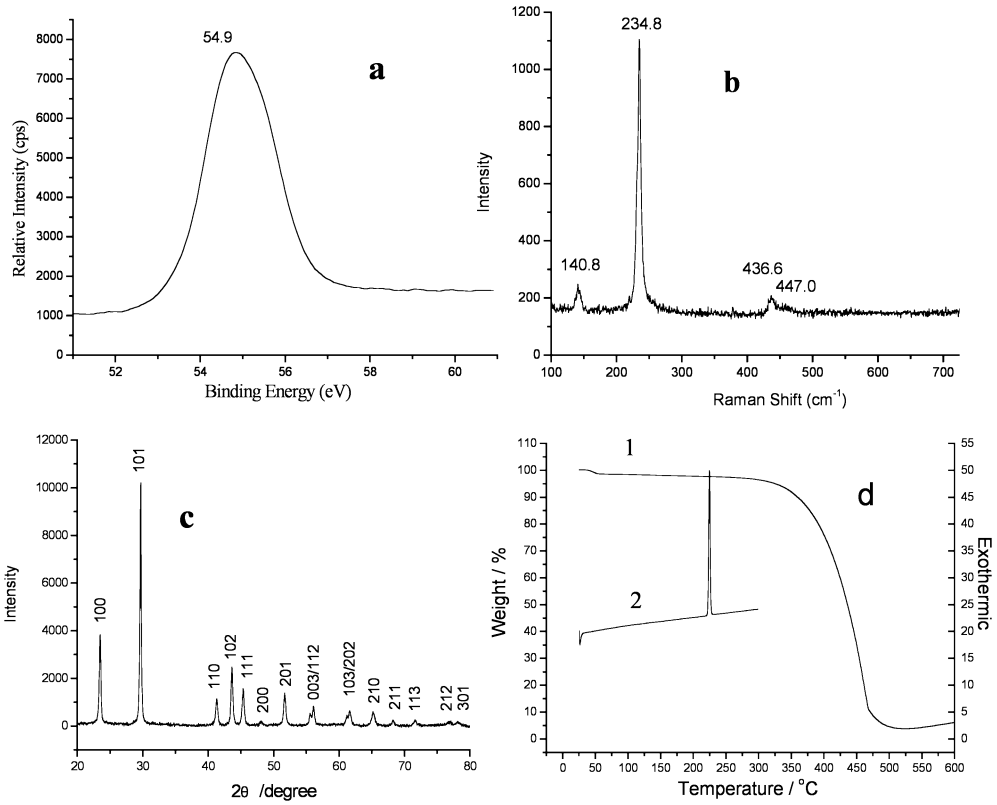

Figure 2. Patterns recorded from a few Se nanotubes: (a) the XPS pattern; (b) the LRS pattern; (c) the XRD pattern; (d) the TG and DSC curves.

of the (001) planes. From the TG curve (curve 1 in Figure 2d) of the Se nanotubes, it can be seen that the mass of the sample remains nearly constant in the range of 100−300 °C, and then the mass decreases sharply to ca. zero upon heating over 450 °C due to the sublimation of elemental Se. The DSC curve (curve 2 in Figure 2d) of the Se nanotubes exhibits an endothermic peak at 224.7 °C, which is assigned to the melting point of the sample since the sample has no loss or gain of mass at this temperature (as shown in curve 1). This melting point is close to that (∼221 °C) of the bulk t-Se[36] but far from that of monoclinic Se (∼175 °C) and a-Se (∼70 °C). Besides, the single narrow DSC peak attests to the uniformity of the sample. Apparently, these results support that the product is made of uniform t-Se nanotubes. In addition, the heat content (enthalpy), which may result from the conversion process of t-Se to the a-Se phase, is calculated from the DSC peak to be 5.82 kJ/mol, which is less than the transformation energy (6.63 kJ/mol) of a-Se to the t-Se phase in bulk. The low enthalpy value of the sample shows the size effect of nanoparticles.

Formation Mechanism. It is well known that surfactant molecules are able to organize themselves into a variety of micelles when their concentration reaches a critical value.[37,38] These micelles can facilitate the formation of nanostructures with special morphologies.[39−42] On the basis of this principle, the possible formation mechanism of our Se nanotubes is speculated in the following section.

In highly concentrated CTAB solution, large amounts of the micelles were formed by the hydrophobic interaction of CTAB molecules.[43] Since CTAB is ionized completely in aqueous systems, the micelles filled with alkyl chains bring along many positive charges in their polar shell. In the synthesis process, the selenious acid radicals with negative charges were first absorbed on the surface of the micelles by electrostatic force and then reduced to elemental Se in situ when the hydrazine was added. Prior to the aging process, some nascent Se particles (mainly a-Se) were quickly transformed into crystal t-Se seeds under ultrasonic irradiation.[18] These t-Se seeds can spontaneously grow along the *c*-axis due to the inherently anisotropic structure of t-Se, accompanied by the dissolution of a-Se colloids in solution according to the Stranski rule.[44] However, the growth of t-Se seeds through the solid−solution−solid process would be limited because there were few a-Se colloids in solution, whereas a large amount of a-Se existed in the polar shell of the CTAB micelles, which have a good ability to solubilize a-Se.[24] Thus, further addition of a few Se atoms to the seed surface would preferentially occur at the edges of the t-Se seeds since these sites had relatively higher free energies.[4] On the basis of the growth along the edges of the t-Se seeds, t-Se nanotubes were gradually formed.

It is worthy of pointing out that the pattern of the t-Se nanotubes is a faceted hexagonal prism rather than a cylinder (as shown in Figure 1b), which was also observed in a few reports.[23,24] Lee and co-workers proved that the crystallographic phase of the initial seed is one of the critical factors for shape determination of the nanocrystals.[45] Tenne found that the faceted instead of cylindrical geometry seems to be a characteristic feature for nonlayered materials.[46] As a nonlayered material, t-Se is composed of helical chains that are formed by a period of three Se atoms.[47] Geometrically, the trigonal frame is the basic cell of the hexagonal frame. Energetically, t-Se hexagonal nanotube rather than the cylindrical nanotube is the most stable shape because this specific nanostructure can give the smallest atom bond angle variation with the lowest strain energy, as confirmed in similarly faceted AlN nanotubes.[48] Thus, the faceted t-Se nanotubes with hexagonal cross sections can be naturally formed through the spiral growth of t-Se seeds along the *c*-axis.

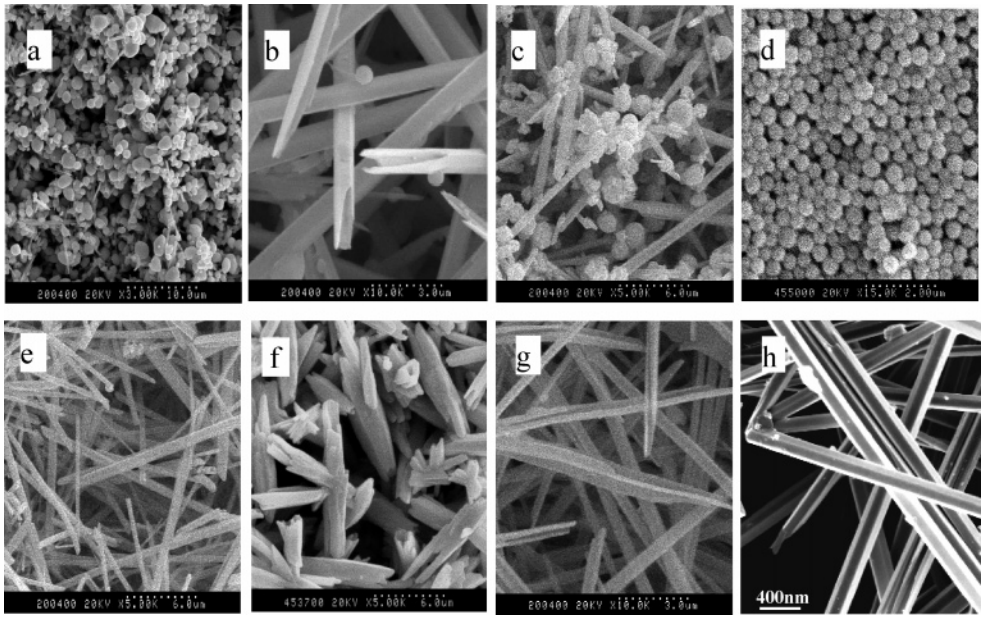

Figure 3. Scanning electron microscopy images of the products obtained under different conditions: (a) without CTAB; (b) in 0.1 M CTAB solution; (c) in solution containing 50% alcohol; (d) in pH 1 solution; (e) in pH 9 solution; (f) the solution aged under ultrasonic irradiation; (g) with a short aging time (1.5 h); (h) the Se nanotubes that had been incubated in water for 3 months (the whole image is shown as Figure 2S in the Supporting Information).

To study the formation mechanism as discussed above, a series of experiments with CTAB solution were performed, and the results are given in Figure 3. In the presence of a low concentration of CTAB or the absence of CTAB, spherical nanoparticles were mainly produced (Figure 3a) since there was a large amount of a-Se colloids in solution. It was found that Se nanotubes were obtained only if the CTAB concentration was equal to or greater than 0.1 M (Figure 3b). These results imply that the highly concentrated CTAB solution, in which a large amount of micelles was formed and mostly a-Se existed in the polar shell of the micelles, is essential for the formation of Se nanotubes. Figure 3c shows the effect of alcohol on the morphology of the final products. The presence of spherical nanoparticles is ascribed to the destruction of CTAB micelles by the alcohol medium. The effect of the acidity is shown in Figures 3d and 3e. These changes in the morphology may result from the effect of the acidity on both the surface character of the CTAB micelles and the dissolution of a-Se on the surface of the micelles. The experimental results show that the acidity (about pH 6) of the initial CTAB solution itself is suitable for the synthesis of Se nanotubes. The ultrasonic irradiation can drive the nucleation of t-Se nanocrystallites,[15] but short nanorods were produced (Figure 3f) if ultrasonic irradiation was used throughout the aging period. This phenomenon indicates that the 1D structures of the product could be shattered by long-term ultrasonic irradiation.

In the interest of probing the evolution of Se nanotubes, the semifinished product was separated from the reaction solution. The presence of semiclosed tubular structures (Figure 3g) suggests that the growth of t-Se seeds along the *c*-axis based on strong covalent bonds is faster than that along the circumferential direction based on weak van der Waals interactions between t-Se helical chains. On the basis of these raw structures, the hexangular nanotubes were gradually formed by following a folding growth mechanism. This weak van der Waals function in the circumferential direction is further disclosed by a phenomenon where a few semiclosed nanotubes (Figure 3h) are produced after the Se nanotubes were incubated in water.

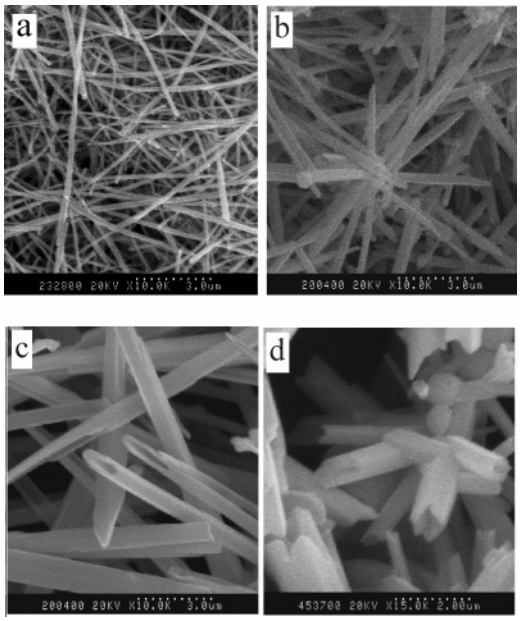

Figure 4. Scanning electron microscopy images of the products obtained at different temperatures: (a) at room temperature; (b) at 40 °C; (c) at 80 °C; (d) at 95 °C.

Apart from the function of CTAB micelles, the temperature of the system plays an important role in the synthesis of Se nanotubes. The dependence of product morphology on the temperature is shown in Figure 4. At low temperatures, only the amorphous particles were produced during the aging time (3 h), and nanorods but not nanotubes could be obtained by a long growth period (Figures 4a and 4b, by aging 3 months and 6 h, respectively). This phenomenon results from the low growth rate of the t-Se seeds at a low temperature. When the temperature was higher, thick-walled nanotubes or multiple short nanotubes were produced in a short time (Figures 4c and 4d, both by aging 2 h) since the high temperature could affect both the function of the CTAB micelles and the mode of t-Se seed growth. The experimental results indicate that 70 °C, close to the melting

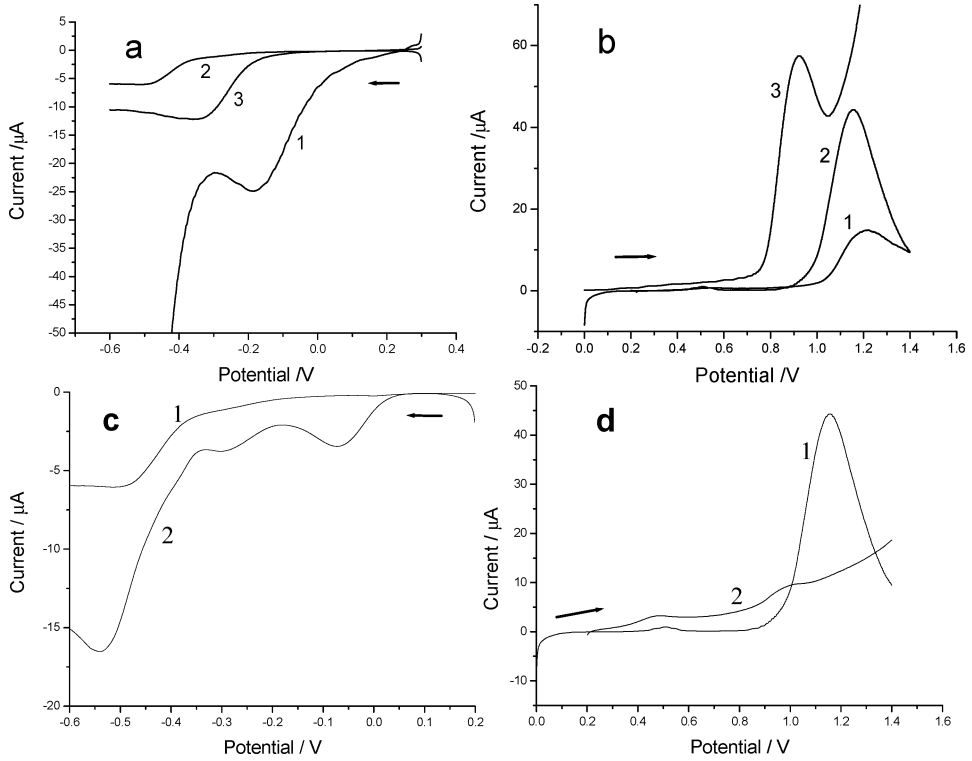

Figure 5. (a) Reduction curves and (b) oxidation curves of the t-Se nanotubes. The electrolytes are 2 M H_2SO_4 (curve 1), 0.1 M KCl (curve 2), and 0.2 M NaOH (curve 3), respectively. (c) Reduction curves and (d) oxidation curves of the t-Se nanotubes (curve 1) and the t-Se in bulk (curve 2) in 0.1 M KCl.

point of a-Se, is the optimal temperature for the synthesis of t-Se nanotubes. Furthermore, as a virtue of this temperature, the high density of the reactants on the surfaces of the CTAB micelles made the synthesis rapid and the yield high.

Electrochemistry. There have been several reports about the electroactivity of elemental Se; however, the conclusions of the reports are disputed.[49] According to the result reported in the literature,[50] elemental Se is very stable and only reduced to Se(II) at −0.4 V, oxidized to Se(IV) at +0.8 V, and then to Se(VI) at +1.2 V in an acidic medium. Figure 5 shows our results for the t-Se nanotubes with a glassy carbon electrode by linear sweep voltammetry. From the voltammograms, it can be seen that the reduction and oxidation features of the t-Se nanotubes were strongly affected by the acidity of the electrolyte solution. The t-Se nanotubes were reduced more easily in acidic solution (the corresponding peak at −0.18 V, as shown in Figure 5a) than in other solutions, since the reduction reaction, $Se(0) + 2H^+ + 2e^- = H_2Se$, can be advanced by H^+. The reduction current increased rapidly at about −0.4 V (curve 1 in Figure 5a), which corresponds to the reduction of H^+. The t-Se nanotubes were oxidized more easily in alkaline solution (the corresponding peak at +0.90 V, as shown in Figure 5b) than in other solutions, since the oxidation reaction, $Se(0) + 5OH^- = HSeO_3^- + 2H_2O + 4e^-$, can be advanced by OH^-. The further oxidation of Se(IV) to Se(VI) took place over +1.2 V (curve 3 in Figure 5b). For comparison, the electrochemical behavior of t-Se in bulk was studied. From Figures 5c and 5d, it can be seen that the t-Se nanotubes were more difficult to reduce and oxidized more easily than t-Se in bulk. The several reduction peaks of t-Se in bulk may result from the different size grains.

The electrochemical behavior of the t-Se nanotubes was further studied by cyclic voltammetry in alkaline solution. From Figures 6a and 6b, it can be seen that there are different oxidation peaks and similar reduction peaks under different sweep modes. Sweeping positively from an initial potential of 0 V and then cyclic sweeping, we observed a single oxidation peak (at +0.92 V on segment 1, Figure 6a). When the experiment was performed by sweeping negatively from an initial potential of +0.30 V and then cyclic sweeping, two oxidation peaks (on segment 2, Figure 6b) were observed, which suggested that Se(0) may exist as two states. On the basis of the previous report that red Se (a-Se) was more difficult to oxidize than gray Se (crystal Se) on a carbon paste electrode,[45] we speculate that the first peak (at +0.93 V) corresponds to the oxidation of the t-Se nanotubes and the second peak (at +1.07 V) is due to the oxidation of a-Se nanoparticles. Besides, in comparison with Figure 6a, it can be observed that the oxidation peak in Figure 6b has a nonsmooth features that may come from the poor conductivity of a-Se nanoparticles. More abnormally, the cathodal curve has an anodic peak (segment 3 in Figure 6b) that may have resulted from the oxidation of interior a-Se nanoparticles as observed in the oxidation curve of the silicon electrode.[51] Here, the a-Se nanoparticles on the surface of electrode had been produced through a conversion process in which t-Se was first reduced to Se(II) in sweeping negatively from +0.3 V (segment 1), and then Se(II) was oxidized to Se(0) (a-Se) when sweeping positively from −0.6 V (segment 2). To confirm our speculation, the a-Se nanoparticles prepared by the reaction of H_2SeO_3 with N_2H_4 in pure water were freshly used in the electrochemical test. As expected, the oxidation peak of the a-Se nanoparticles is at +1.05 V in alkaline solution, whereas that of Se nanotubes is at +0.92 V under the same conditions.

Although the speculation has been confirmed, the present results for the electroactivity of the two Se states are in disagreement with those observed on an Au electrode in our previous work,[26] which drove us to reexamine the characteristics of the two Se states. We think that the strong sorption of both the a-Se nanoparticles and the carbon electrode made the oxidation of a-Se nanoparticles more difficult than that of Se

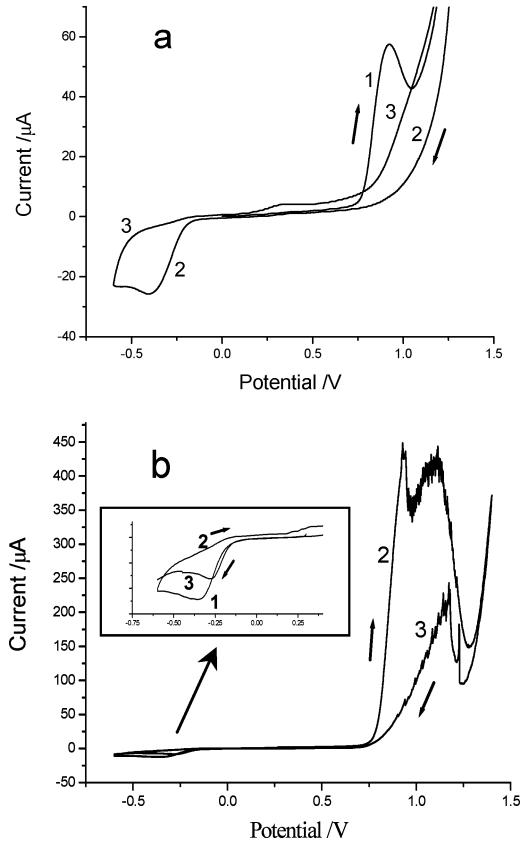

Figure 6. Cyclic voltammograms of the Se nanotubes, obtained by different sweeping modes in 0.2 M NaOH: (a) first sweeping positively from an initial voltage of 0 V; (b) first sweeping negatively from an initial voltage of +0.3 V. (Arabic numerals indicate the sequence of the scan segments.)

nanotubes on glassy carbon electrodes in alkaline solution. In addition, it has been observed that a-Se nanoparticles could not be oxidized on glassy carbon electrodes in 0.1 M KCl solution until the potential went up to +1.3 V (Figure 3S in the Supporting Information).

Conclusions

In summary, faceted single-crystalline Se nanotubes with diameters around 300 nm (wall thicknesses of 60 nm) and lengths up to 100 μm were rapidly synthesized on a large scale (gram quantities). The results of the measurements indicate that the nanotubes are made up of a pure trigonal phase of Se and the growth direction of the nanotubes is along the *c*-axis of t-Se. On the basis of a series of the SEM observations, it is proposed that the CTAB micelles and the reaction temperature are essential in the synthesis. From the energetics and geometry, it is demonstrated that the faceted model for t-Se nanotubes is a more favorable nanostructure. In addition, the results of electrochemical experiments show that the electroactivity of t-Se nanotubes, which was strongly affected by the acidity of the electrolyte solution, is different from that of a-Se nanoparticles and t-Se in bulk. It should be pointed out that the t-Se nanotubes may be useful as components in constructing the photoelectronic devices and as templates in constructing other 1D nanostructures. The as-observed redox characteristics of t-Se nanotubes are significant in a variety of diverse fields.

Acknowledgment. Support for this work from the National Natural Science Foundation of China (Grant Nos. 90206037, 20521503, and 20435010) and the Jiangsu Scientific Project (BK2004210) is gratefully acknowledged.

Supporting Information Available: The EDAX of the Se nanotubes, the SEM image of the product after incubation in water for 3 months, and the cyclic voltammogram of the a-Se nanoparticles. This material is available for free of charge via the Internet at http://pubs.acs.org.

References and Notes

(1) Iijima, S. *Nature* **1991**, *354*, 56−58.
(2) Seo, D. S.; Lee, K. H.; Kim, H. J. *J. Cryst. Growth* **2001**, *229*, 428−432.
(3) Zhang, Y. X.; Li, G. H.; Zhang, L. D. *Chem. Lett.* **2004**, *33*, 334−335.
(4) Mayers, B.; Xia, Y. N. *Adv. Mater.* **2002**, *14*, 279−282.
(5) Yang, Z. H.; Gu, Y. L.; Chen, L. Y.; Shi, L.; Ma, J. H.; Qian, Y. T. *Solid State Commun.* **2004**, *130*, 347−351.
(6) Remskar, M.; Mrzel, A.; Skraba, Z.; Jesih, A.; Ceh, M.; Demsȳar, J.; Stadelmann, P.; Levy, F.; Mihailovic, D. *Science* **2001**, *292*, 479−481.
(7) Zhang, H.; Ma, X. Y.; Xu, J.; Yang, D. R. *J. Cryst. Growth* **2004**, *263*, 372−376.
(8) Spahr, M. E.; Bitterli, P.; Nesper, R.; Kruunimeich, F.; Nissen, H. U. *Angew. Chem., Int. Ed.* **1998**, *37*, 1263−1265.
(9) Wang, Y. H.; Ye, C. H.; Zhang, L. D. *Chem. Lett.* **2004**, *33*, 166−167.
(10) Wu, Q.; Hu, Z.; Wang, X. Z.; Lu, Y. N.; Chen, X.; Xu, H.; Chen, Y. *J. Am. Chem. Soc.* **2003**, *125*, 10176−10177.
(11) Johnson, J. A.; Saboungi, M. L.; Thiyagarajan, P.; Csencsits, R.; Meisel, D. *J. Phys. Chem. B* **1999**, *103*, 59−63.
(12) Cui, Y.; Wei, Q. Q.; Park, H. K.; Lieber, C. M. *Science* **2001**, *293*, 1289−1292.
(13) Gates, B.; Yin, Y.; Yang, P.; Xia, Y. N. *J. Am. Chem. Soc.* **2001**, *123*, 11500−11501.
(14) Mayers, B.; Jiang, X.; Sunderland, D.; Cattle, B.; Xia, Y. N. *J. Am. Chem. Soc.* **2003**, *125*, 13364−13365.
(15) Gates, B.; Mayers, B.; Grossman, A.; Xia, Y. N. *Adv. Mater.* **2002**, *14*, 1749−1752.
(16) Gates, B.; Mayers, B.; Cattle, B.; Xia, Y. N. *Adv. Funct. Mater.* **2002**, *12*, 219−227.
(17) Zhang, X.; Xie, Y.; Xu, F.; Liu, X. H.; Zhang, S. Y.; Tian, X. B. *Solid State Sci.* **2003**, *5*, 525−527.
(18) Mayers, B.; Liu, K.; Sunderland, D.; Xia, Y. N. *Chem. Mater.* **2003**, *15*, 3852−3858.
(19) An, C. H.; Tang, K. B.; Liu, X. M.; Qian, Y. T. *Eur. J. Inorg. Chem.* **2003**, 3250−3255.
(20) Zhu, Y. J.; Hu, X. L. *Mater. Lett.* **2004**, *58*, 1234−1236.
(21) Wang, X. J.; Zheng, X. W.; Lu, J.; Xie, Y. *Ultrason. Sonochem.* **2004**, *11*, 307−310.
(22) Zhang, H.; Zuo, M.; Tan, S.; Li, G. P.; Zhang, S. Y.; Hou, J. G. *J. Phys. Chem. B* **2005**, *109*, 10653−10657.
(23) Zhang, H.; Yang, D. R.; Ji, Y. J.; Ma, X. Y.; Xu, J.; Que, D. L. *J. Phys. Chem. B* **2004**, *108*, 1179−1182.
(24) Ma, Y. R.; Qi, L. M.; Ma, J. M.; Cheng, H. M. *Adv. Mater.* **2004**, *16*, 1023−1026.
(25) Li, X. M.; Li, Y.; Li, S. Q.; Zhou, W. W.; Chu, H. B.; Chen, W.; Li, I. L.; Tang, Z. K. *Cryst. Growth Des.* **2005**, *5*, 911−916.
(26) Zhang, S. Y.; Zhang, J.; Liu Y.; Ma X.; Chen, H. Y. *Electrochim. Acta* **2005**, *50*, 4365−4370.
(27) Pandy, R. K.; Sahu, S. N.; Chandra, S. *Handbook of Semiconductor Electrodeposition*; Marcel Dekker: New York, 1996.
(28) Ferri, T.; Sangiorgio, P. *Anal. Chim. Acta* **1999**, *385*, 337−343.
(29) Gates, B.; Yin, Y.; Xia, Y. N. *J. Am. Chem. Soc.* **2000**, *122*, 12582−12583.
(30) Gao, X.; Zhang, J.; Zhang, L. *Adv. Mater.* **2002**, *14*, 290−293.
(31) Wang, D. B.; Yu, D. B.; Mo, M. S.; Liu, X. M.; Qian, Y. T. *J. Cryst. Growth* **2003**, *253*, 445−451.
(32) Ren, L.; Zhang, H. Z.; Tan, P. H.; Chen, Y. F.; Zhang, Z. S.; Chang, Y. Q.; Xu, J.; Yang, F. H.; Yu, D. P. *J. Phys. Chem. B* **2004**, *108*, 4627−4630.
(33) Weser, U.; Sokolowski, G.; Pilz, W. *J. Electron Spectrosc.* **1977**, *10*, 429.
(34) Lucovsky, G.; Mooradian, A.; Taylor, W.; Wright, G. B.; Keezer, R. C. *Solid State Commun.* **1967**, *5*, 113.
(35) Stuke, J. In *Selenium*; Zingaro, R. A., Cooper, W. C., Eds.; Van Nostrand Reinhold: New York, 1974.
(36) Zhu, Y. J.; Hu, X. L. *Mater. Lett.* **2004**, *58*, 1234−1236.
(37) Zielinski, R.; Ikeda, S.; Nomura, H.; Kato, S. *J. Colloid Interface Sci.* **1988**, *125*, 497−507.
(38) Ringsdorf, H.; Schlarb, B.; Venzmer, J. *Angew. Chem., Int. Ed. Engl.* **1988**, *27*, 113−158.
(39) Nikhil, R. J.; Latha, G.; Catherine, J. M. *Chem. Commun.* **2001**, 617−618.

(40) Nikhil, R. J.; Latha, G.; Catherine, J. M. *J. Phys. Chem. B* **2001**, *105*, 4065−4067.
(41) Murphy, C. J.; Jana, N. R. *Adv. Mater.* **2002**, *14*, 80−82.
(42) Xia, Y. N.; Yang, P.; Sun, Y.; Wu, Y.; Mayers, B.; Gates, B.; Yin, Y.; Kim, F.; Yan, H. *Adv. Mater.* **2003**, *15*, 353−389.
(43) Tornblom, M.; Henriksson, U. *J. Phys. Chem. B* **1997**, *101*, 6028−6035.
(44) Jolivet, J. P.; Henry, M.; Livage, J. *Metal Oxide Chemistry and Synthesis—From Solution to Solid State*; Bescher, E., Translator; John Wiley and Sons: Chichester, U. K., 2000.
(45) Lee, S. M.; Cho, S. N.; Cheon, J. *Adv. Mater.* **2003**, *15*, 441−444.
(46) Tenne, R. *Angew. Chem., Int. Ed.* **2003**, *42*, 5124−5132.
(47) Tani, Y.; Shirakawa, Y.; Shimosaka, A.; Hidaka, J. *J. Non-Cryst. Solids* **2001**, *293−295*, 779−784.
(48) Chen, X.; Ma, J.; Hu, Z.; Wu, Q.; Chen, Y. *J. Am. Chem. Soc.* **2005**, *127*, 7982−7983.
(49) Espinosa, A. M.; Tascon, M. L.; Vazquez, M. D.; Batanero, P. S. *Eletrochim. Acta* **1992**, *37*, 1165−1172.
(50) Pourbaix, M. *Atlas d'Équilibres É*Electrochimiques; Gauthier-Villars: Paris, 1963.
(51) Xia, X. H.; Kelly, J. J. *Electrochim. Acta* **2000**, *45*, 4645−4653.